Journal of Magnetism and Magnetic Materials 466 (2018) 306–310

Contents lists available at ScienceDirect

Journal of Magnetism and Magnetic Materials

journal homepage: www.elsevier.com/locate/jmmm

Research articles

Local iron ion distribution and magnetic properties of the perovskites $La_{1-x}Sr_xFeO_{3-\gamma}$.

R.B. da Silva[a,*], J.M. Soares[a], José. A.P. da Costa[a], J.H. de Araújo[b], A.R. Rodrigues[c], F.L.A. Machado[c]

[a] Departamento de Física, Universidade do Estado do Rio Grande do Norte, 59610-010 Mossoró, RN, Brazil
[b] Departamento de Física Teórica e Experimental, Universidade Federal do Rio Grande do Norte, 59072-970 Natal, RN, Brazil
[c] Departamento de Física, Universidade Federal de Pernambuco, 50670-901 Recife, PE, Brazil

ARTICLE INFO

Keywords:
Sol gel method
Orthoferrites
Hexaferrites
Magnetic properties
Mössbauer spectroscopy

ABSTRACT

The influence of thermal annealing on the structural and magnetic properties of nanocrystalline $La_{1-x}Sr_xFeO_{3-\gamma}$ perovskites with $x = 0$, 0.3, 0.4 and 0.5 was investigated by X-ray diffraction (XRD), scanning electron microscopy (SEM), Mössbauer spectroscopy and magnetization measurements. Samples prepared by a sol gel method were calcined for 4 h at 1073 K and annealed for 8 h at 1273 K. XRD data indicate the formation of single phases in all samples, orthorhombic with the space group Pbnm for $x = 0.0$ and 0.3 and rhombohedral with the space group $R\bar{3}c$ for $x = 0.4$ and 0.5. The Mössbauer spectroscopy reveal that the sintering process increase the amount of Fe^{4+} and decrease the paramagnetic sites. Despite of the XRD data indicating the samples to be single phase, the higher coercivity observed in the samples with $x = 0.4$ may be associated with the emergence of $Sr_{1-x}La_xFe_{12}O_{19}$ clusters in the samples. Irreversibility in the measurements of magnetization as a function of temperature was interpreted in terms of a high temperature glass cluster behavior.

1. Introduction

In the last decade, the perovskites $La_{1-x}Sr_xFeO_{3-\gamma}$ (LSFO) with $0 \leqslant x \leqslant 1$ have attracted considerable attention for presenting a wide range of interesting physical properties [1–4]. LSFO has also being investigated because of its potential in technological applications. For instance, LSFO has been used as oxygen storage material (OSM) [5] and as membrane material in partial oxidation of methane (POM) reactors with planar and tubular designs, yielding high values for CO selectivity and CH_4 conversion [6,7].

Compounds with composition ABO_3, where *A* are rare earth elements and *B* are metals, were found to have perovskite-like crystalline structures. When the metallic ion (B) is Fe resulting $AFeO_3$, the compounds are named orthoferrites and their perovskite structure becomes distorted. The orthoferrites have also been extensively studied lately. Among them, $LaFeO_3$ (LFO) has an orthorhombic structure with a space group Pbmn. This compound is an antiferromagnetic insulator with a Néel temperature (T_N) of about 740 K [8]. $SrFeO_3$ (SFO) is also a well known orthoferrite but this compound is metallic with $T_N = 134$ K and it has a cubic symmetry with a space group Pm-3 m [8,9]. The divalent ions Sr^{2+} in SFO were found to be readily replaced by trivalent ions of lanthanum (La^{3+}) yielding the mixed orthoferrites $La_{1-x}Sr_xFeO_{3-\gamma}$. The replacement of La^{3+} by Sr^{2+} was found to increase the electronic conduction and to decrease T_N. Another consequence of the ionic substitution of La^{3+} by Sr^{2+} is an increase in valence state of Fe ions since it is trivalent (Fe^{3+}) in $LaFeO_3$ and tetravalent (Fe^{4+}) in the $SrFeO_3$. Thus, the replacement of La by Sr to produce $La_{1-x}Sr_xFeO_{3-\gamma}$ result in a mixed valence of the Fe^{3+} and Fe^{4+} ions and such compounds are named mixed valence oxides [10]. A weak ferromagnetism with a spontaneous magnetization that decreases with increasing amount of Sr was observed in samples with compositions in the range $0 \leqslant x \leqslant 0.3$ [11]. For $x = 2/3$ a charge order (CO) phenomenon has been observed below a Verwey transition temperature (T_V) of 210 K [12,13]. A disproportion of charges occurs in the sites with Fe ions leading to the paramagnetic state with a net ionic valence of $Fe^{+3.65}$. Moreover, a mixing of $2Fe^{3+}$ and Fe^{5+} was found in the antiferromagnetic CO state below T_V yielding an ionic iron sequence of $Fe^{3+}Fe^{3+}Fe^{5+}Fe^{3+}Fe^{3+}$…along the [1 1 1] direction of the Perovskite unit cell [2,3,14]. The interactions between pairs of Fe^{3+}–Fe^{3+} are of the super exchange type that leads to antiferromagnetic interaction (J_{AF}) while between pairs of Fe^{3+}–Fe^{5+} the nature of the interaction is ferromagnetic (J_F)[2,14]. Inelastic neutron scattering (INS) has been used for determining the values of both J_F and J_{AF} and it was observed that, depending on the ratio J_F/J_{AF}, a CO state may be stabilized by the magnetic interactions [2].

* Corresponding author.
E-mail address: rodolfo.bezerra.silva@gmail.com (R.B. da Silva).

https://doi.org/10.1016/j.jmmm.2018.07.040
Received 11 April 2018; Received in revised form 23 June 2018; Accepted 11 July 2018

Polycrystalline $La_{1-x}Sr_xFeO_{3-\gamma}$ samples with a broad range of particle size (80–2000 nm) were investigated by magnetization and specific heat measurements [3]. The authors found that the CO state may be suppressed by reducing the size of the particle. Moreover, a weak ferromagnetism and high coercive fields have been revealed by magnetic measurements at room temperature for samples with diameter less than 300 nm. The catalytic properties of high purity $La_{1-x}Sr_xFeO_{3-\gamma}$ with $0 \leqslant x \leqslant 0.5$ were also found to be strongly influenced by the substitution of La by Sr [6].

On synthesis of these materials, deviation from nominal composition may cause formation of secondary phases. Even a small amount of secondary phases can be critical in preparation of dense ceramic and may influence its electrical, magnetic and catalytic properties. In this work, powder samples of $La_{1-x}Sr_xFeO_{3-\gamma}$ ($0.3 \leqslant x \leqslant 0.5$) (LSFO) have been synthesized with different average particle sizes using a sol gel (SG) method. The samples were characterized by X-ray diffraction (XRD), scanning electron microscopy (SEM), Mössbauer spectroscopy and magnetic measurements. A weak ferromagnetism was observed in the samples with x = 0.3 and 0.5. A coercivity substantially higher than those previously reported was also observed for a sample composition with x= 0.4. The enhancement in the coercivity was associated with traces of $SrFe_{12}O_{19}$ present in the sample investigated in the present work.

2. Experimental

Powder samples of $La_{1-x}Sr_xFeO_{3-\gamma}$ with $0 \leqslant x \leqslant 0.5$ were prepared by a sol-gel method by using high purity lanthanum nitrate $La(NO_3)_3$. $6H_2O$, strontium nitrate $Sr(NO_3)_2$ and iron nitrate $Fe(NO_3)_3$. $9H_2O$, ethylene glycol and acid citric [15]. After the samples were synthesized, the powders were taken to a furnace for heat treatments. First, the samples were calcined at 1073 K for 4 h and later they were sintered at 1273 K for 8 h under a flow of O_2. X-ray diffraction (XRD) patterns were obtained by using Cu-Kα radiation in a Rigaku bench diffractometer model Mine Flex II. The XRD data were collected using a scan rate of 2°/min in steps of 0.02°. The structural parameters and the average particle size were obtained by using the MAUD code and Rietveld refinement [16]. The morphology and microstructure of the samples were investigated making use of scanning electron microscopy (SEM) images obtained in a Shimadzu Tescan Mira 3 Microscope. Mössbauer spectroscopy was performed at room temperature using a constant acceleration Mössbauer spectrometer operating in a triangular wave mode and a ^{57}Co source embedded in a rhodium matrix. A 25 μm thick α-Fe sheet was used for calibrating the Mössbauer spectrometer. Finally, the magnetic data was obtained by using a vibrating sample magnetometer (VSM).

3. Results and discussion

3.1. XRD and SEM

X-ray diffraction (XRD) patterns for calcined only samples (calc) and for samples that were also sintered (sint) are shown in Fig. 1. The Rietveld refinement applied to the XRD spectra showed that the samples are orthorhombic with a space group Pbnm for $x = 0$ and 0.3 and they are rhombohedral with a space group R$\bar{3}$c for $x = 0.4$ and 0.5.

The parameters obtained from the Rietvield refinement for the sintered samples are listed in Table 1. The average particle sizes D_m of the crystallites were found first to decrease for increasing concentrations of Sr, ranging from $D_m = 118.8$ nm at $x = 0$ to $D_m = 67.9$ nm for $x = 0.4$, but then increase to $D_m = 106.5$ nm for $x = 0.5$. These results are in accordance to those reported by Jiangong li et al. [11], even though the sample with x = 0.4 yielded a better refinement for rhombohedral symmetry and space group R$\bar{3}$c. Moreover, for the sample with $x = 0.5$ a good refinement was only achieved by using a mixture of two phases: an orthorhombic (space group Pbnm) and a R$\bar{3}$c rhombohedral

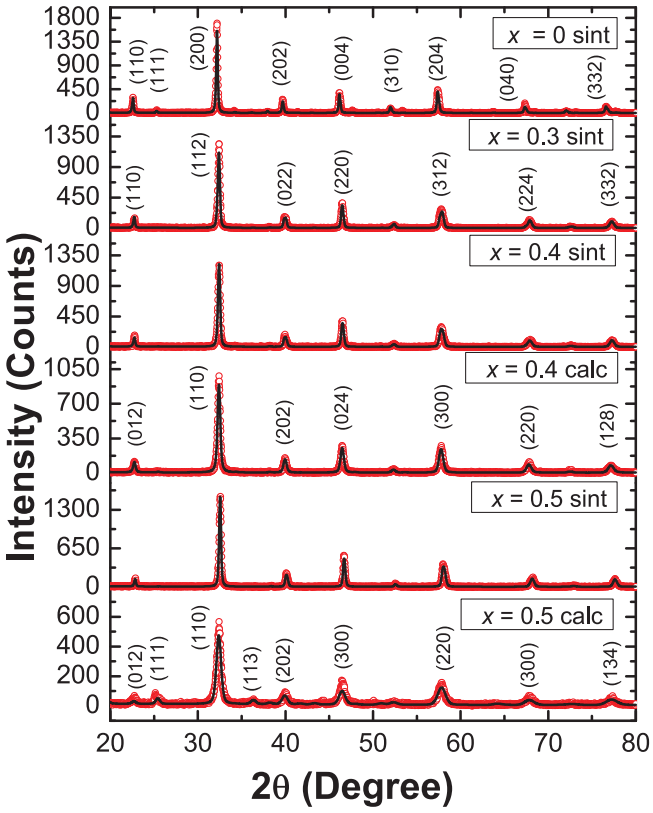

Fig. 1. XRD patterns for samples of $La_{1-x}Sr_xFeO_{3-\gamma}$ ($0 \leqslant x \leqslant 0.5$).

Table 1
Concentration of Sr, mean diameter D_m (nm), symmetry, space group and lattice parameters of samples $La_{1-x}Sr_xFeO_{3-\gamma}$ ($0 \leqslant x \leqslant 0.5$).

Sr	D_m (nm)	Symmetry	Lattice Parameters (Å)
x = 0.0	118.8	Orthorhombic Pbnm	(a) = 5.5 (b) = 5.5 (c) = 7.8
x = 0.3	100	Orthorhombic Pbnm	(a) = 5.5 (b) = 5.5 (c) = 7.7
x = 0.4	67.9	Rhombohedral R$\bar{3}$c	(a) = 5.5 (c) = 13.4
x = 0.5	106.4	Rhombohedral R$\bar{3}$c	(a) = 5.5 (c) = 13.4

phase. The morphology of the nanoparticles for calcined samples with $x = 0.3$, 0.4 and 0.5 were also investigated by scanning electron microscopy (SEM). The SEM images shown in Fig. 2 indicate that the size of the particles is somewhat homogeneous and the sample with $x = 0.4$ is indeed the one with smaller average particle size.

3.2. Mössbauer spectroscopy

Mössbauer spectroscopy was employed at room temperature for investigating the magnetic ordering in calcined only samples and in samples that were sintered as well. It was found that the overall results are in good agreement with some found in the literature [10,13,17,18]. However, unlike in the XRD data, differences were observed between the Mössbauer spectra for the calcined and for the sintered samples with $x = 0.3$, 0.4 and 0.5. For comparison, Fig. 3 shows a Mössbauer spectrum for a sintered sample of $LaFeO_3$ ($x = 0$) where the typical

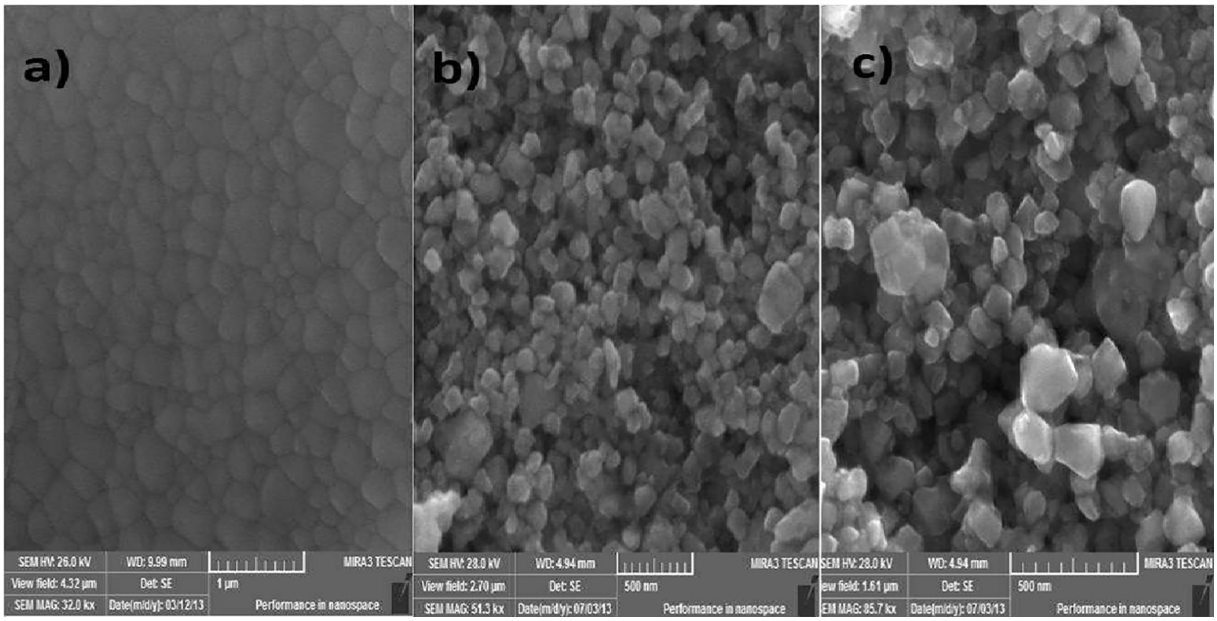

Fig. 2. SEM images of the sinterized $La_{1-x}Sr_xFeO_{3-\gamma}$ ($0.3 \leqslant x \leqslant 0.5$). Images a), b) and c) are for samples $x = 0.3$, $x = 0.4$ and $x = 0.5$, respectively.

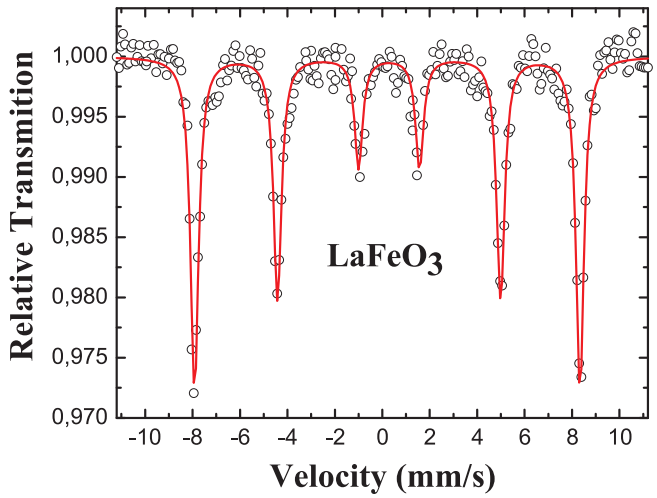

Fig. 3. Mössbauer spectroscopy for the sintered $LaFeO_{3-\gamma}$ sample.

sextet splitting associated to magnetic ordering is observed. For this magnetic moment configuration the number of sites with Fe^{3+} was found to be significant larger than the ones with Fe^{4+}. The hyperfine fitting parameters for $LaFeO_3$ are $H_{hf} = 505.1$ kOe, $\Delta Q = -0.08$ mm/s and $\delta = 0.26$ mm/s, respectively, for the hyperfine magnetic field, quadrupole splitting and chemical shifting parameters.

Fig. 4 shows Mössabuer spectra for calcined samples of $La_{1-x}Sr_xFeO_{3-\gamma}$ for $x = 0.3$, 0.4 and 0.5. The spectra were nicely fit by using six sub-spectra: one singlet and one doublet associated to two paramagnetic sites and four sextets associated to the magnetically ordered phases and to the iron oxidation states Fe^{3+} and Fe^{4+}, distributed in three non equivalent sites. The Mössabuer spectra for the sintered samples are shown in Fig. 5. The spectra for the samples with $x = 0.3$ and 0.4 were adjusted by using similar fitting parameters and slightly varying the relative absorption area (A). Again, the magnetically ordered sites were represented by sextets. It is interesting to notice that for the $La_{0.7}Sr_{0.3}FeO_{3-\gamma}$ calcined sample the paramagnetic contributions (represented by singlets and doublets) correspond to about 28.8% while for the sintered sample they only correspond to about 13.7%. A decrease in the paramagnetic contribution with siterization was also observed for the sample with $x = 0.4$. The differences between the values of the

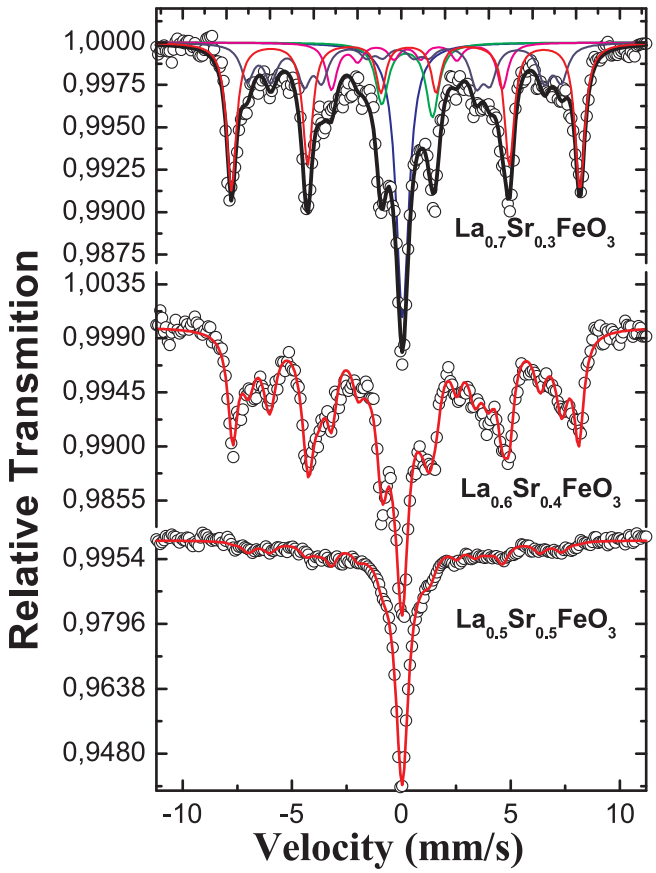

Fig. 4. Room temperature Mössbauer spectra for orthoferrites $La_{1-x}Sr_xFeO_{3-\gamma}$ ($0.3 \leqslant x \leqslant 0.5$) calcined.

hyperfine fields (H_{hf}) and between the quadrupole shifts (ΔQ) are good indicators of the ionic coordination symmetry. The Mössabuer parameters are summarized for both samples, e.g., the calcined samples and the calcined and sintered ones, in Table 2. Since the amount of Fe^{4+} in the calcined sample with x = 0.4 is larger then in one with x = 0.3, the amount of Fe^{3+} is reduced which, in turn, increases the sextet

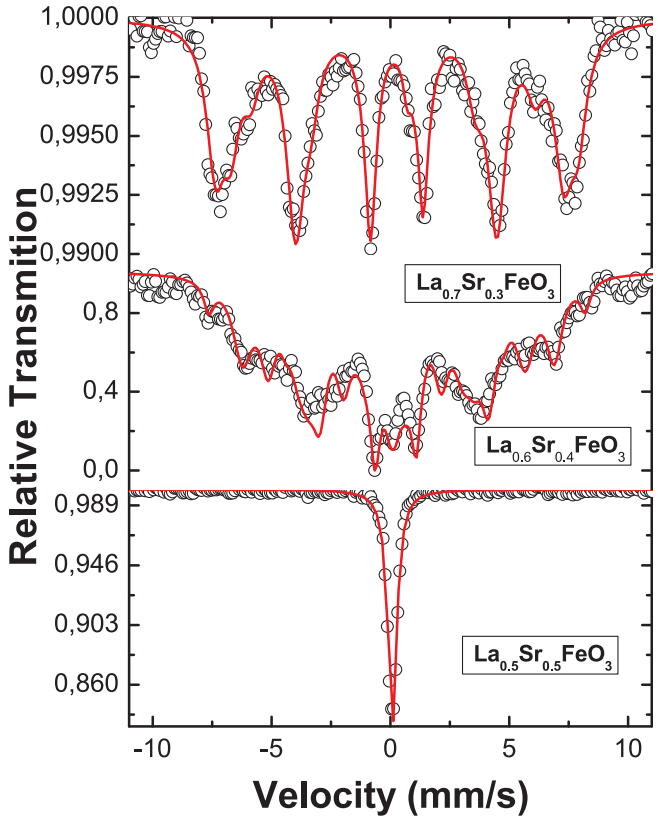

Fig. 5. Mössbauer spectra sintered orthoferrites $La_{1-x}Sr_xFeO_{3-\gamma}$ ($0.3 \leqslant x \leqslant 0.5$).

contribution. For comparison, the paramagnetic contributions decrease from 28.78% for $x = 0.3$ to 27.27% for $x = 0.4$, however for sinterized samples the paramagnetic contribution increased from 13.70% to 23.16%. Obviously, this rule cannot be generalized for all sites since they are randomly filled and the percentage of absorption cannot be assumed to be the same in both cases. Finally, it was necessary to include only small amplitudes for the sextet contribution to obtaining a good fit to the Mössbauer spectrum of the calcined sample with $x = 0.5$.

The difference between the absorption spectra is a clear indication of a redistribution of the iron ions in the crystallographic sites with direct influence on the magnetic properties of the samples. An ionic redistribution is expected, for instance, due to the variation in the amount of oxygen in the sample composition during the sintering process. The sinterization increase the Fe^{4+} absorbtion, for example, the amount of Fe^{4+} increase from 39.70% to 48.95% for x = 0.3 sample and increase from 48.46% to 52.77% for x = 0.4 sample. Thus, as required from the charge balance, an increase in the amount of oxygen leads to an increase in the amount of Fe^{4+} thereby reducing the number of paramagnetic sites. Finally, the Mössbauer spectrum for $x = 0.5$ sintered sample fitted using two singlets only. The singlets are related to the Fe^{3+} and Fe^{4+} iron ions siting on equivalent crystallographic sites.

3.3. Magnetization

Room temperature magnetic hysteresis loops for the perovskite $La_{1-x}Sr_xFeO_{3-\gamma}$ ($0.3 \leqslant x \leqslant 0.5$) calcined and sintered are shown in Fig. 6. A weak ferromagnetism was observed for the calcined sample with $x = 0.3$ and 0.5, whereas for both calcined and sintered samples with $x = 0.4$ an significant increase in the coercivity and saturation magnetization is observed. Similar behavior has been published in literature [3] in studies of the La-Sr-Fe-O system. For instance, for the calcined $La_{0.6}Sr_{0.4}FeO_{3-\gamma}$ sample, the hysteresis curve shows a magnetization measured at the highest applied magnetic field $M(H_{max})$ of 1.41 emu/g and a coercive field of $H_c = 2.8$ kOe, whereas for x = 0.3 and 0.5

Table 2
Mössbauer parameters for calcined and sintered $La_{1-x}Sr_xFeO_{3-\gamma}$ samples and synthesized by SG method. The isomer shift values are relative to metallic α-Fe.

$La_{0.7}Sr_{0.3}FeO_{3-\gamma}$ calcined						
Sites	Fe^{4+}	Fe^{3+}	Fe^{3+}	Fe^{4+}	Fe^{4+}	Fe^{3+}
H_{hf} (KOe)	–	–	248.14	388.34	453.44	496.20
ΔQ (mm/s)	–	2.28	0.40	0.41	0.21	0.10
δ (mm/s)	0.05	0.29	0.48	0.11	0.06	0.25
Γ (mm/s)	0.64	0.45	1.00	0.91	0.85	0.50
A (%)	19.17	9.61	11.34	9.29	10.91	39.68
$La_{0.6}Sr_{0.4}FeO_{3-\gamma}$ calcined						
H_{hf} (KOe)	–	–	244.91	386.63	449.46	492.67
ΔQ (mm/s)	–	2.22	0.53	0.27	0.30	0.14
δ (mm/s)	0.04	0.26	0.55	0.09	0.05	0.27
Γ (mm/s)	0.76	0.41	0.76	1.07	0.97	0.50
A (%)	17.25	10.02	16.03	14.18	17.03	25.49
$La_{0.5}Sr_{0.5}FeO_{3-\gamma}$ calcined						
H_{hf} (KOe)	–	–	235.04	380.78	440.69	483.18
ΔQ (mm/s)	–	2.24	0.58	0.41	0.21	0.10
δ (mm/s)	0.02	0.23	0.61	0.11	0.06	0.25
Γ (mm/s)	0.73	0.45	1.00	0.91	0.85	0.50
A (%)	56.07	7.70	14.62	9.43	8.72	3.46
$La_{0.7}Sr_{0.3}FeO_{3-\gamma}$ sinterized						
H_{hf} (KOe)	–	–	256.92	383.03	445.66	478.03
ΔQ (mm/s)	–	2.19	0.57	0.08	0.06	0.05
δ (mm/s)	0.05	0.28	0.11	0.14	0.17	0.22
Γ (mm/s)	0.64	0.37	0.56	1.13	0.91	0.57
A (%)	< 0.05	13.70	13.08	16.56	32.39	24.27
$La_{0.6}Sr_{0.4}FeO_{3-\gamma}$ sinterized						
H_{hf} (KOe)	–	–	227.19	313.32	394.66	483.32
ΔQ (mm/s)	–	1.81	0.25	0.03	0.40	0.03
δ (mm/s)	0.07	0.23	0.24	0.18	0.07	0.13
Γ (mm/s)	0.76	0.41	0.93	1.05	0.96	0.35
A (%)	8.38	14.78	25.90	20.26	24.13	6.55
$La_{0.5}Sr_{0.5}FeO_{3-\gamma}$ sinterized						
H_{hf} (KOe)	–	–	–	–	–	–
ΔQ (mm/s)	–	–	–	–	–	–
δ (mm/s)	0.02	0.16	–	–	–	–
Γ (mm/s)	0.31	0.32	–	–	–	–
A (%)	49.08	50.92	–	–	–	–

$M(H_{max})$ and H_C values of 0.5 and 0.7 emu/g and 0.20–0.24 kOe, respectively, were observed. Values for $M(H_{max})$ above 0.25 emu/g were obtained by annealing the samples in an atmosphere of CO/CO_2 [18]. The enhancement in $M(H_{max})$ is accounted by the fact that these samples have rhomboedral symmetry with larger Fe-O bond length which, in turn, weakens the superexchange interactions and enhances the ferromagnetic ones. Values for $M(H_{max})$ of 2.38 emu/g and for H_c of 4.6 kOe for sintered samples of $La_{0.6}Sr_{0.4}FeO_{3-\gamma}$ have also been observed.

Fig. 7 shows the temperature dependence of the ZFC and FC magnetization M(T) curves the calcined sample with x = 0.4 measured for two values of applied magnetic fields: 100 and 1000 Oe. We observe a high irreversibility of the ZFC and FC curves with a field dependence of the irreversibility temperature. For a field of the 100 Oe the irreversibility temperature is ~709 K while a field of the 1000 Oe the irreversibility temperature is ~715 K. This is a typical of spin glass like behavior (SG) [19]. The analysis of the data reveals a transition temperature T_c for this sample of around 700 K can be attributed to the

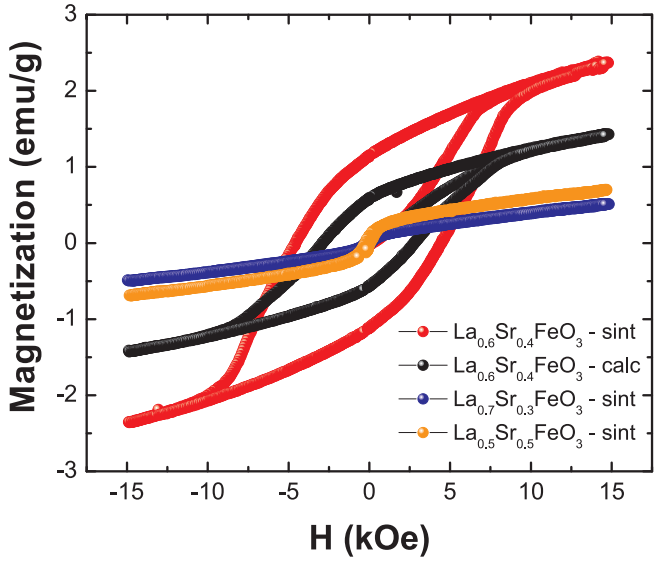

Fig. 6. Magnetization measurements made at 300 K calcined and sintered samples $La_{1-x}Sr_xFeO_{3-\gamma}$ ($0.3 \leqslant x \leqslant 0.5$) produced sol gel method.

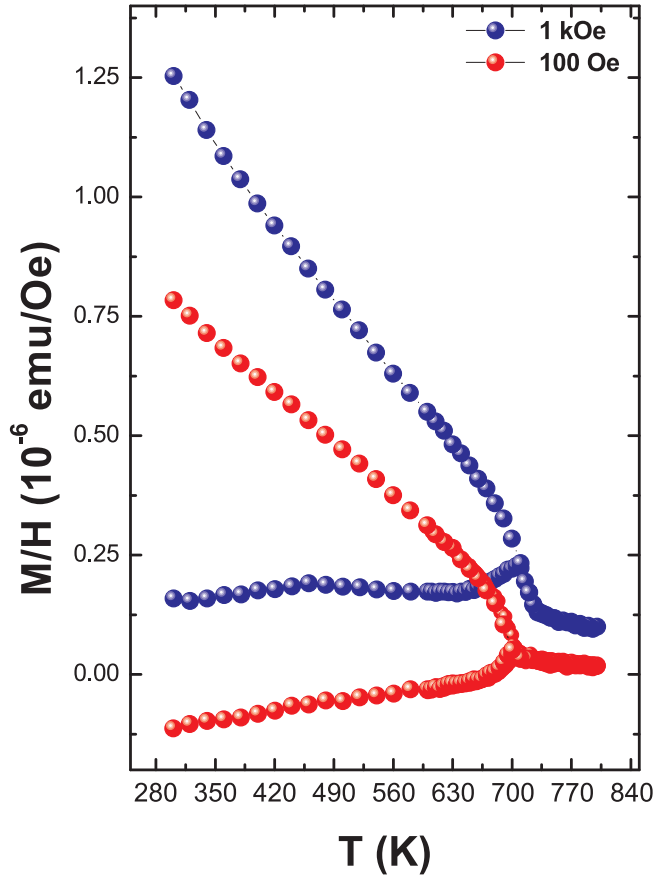

Fig. 7. ZFC and FC curves for $x = 0.4$ calcined sample measured in two distinct fields 100 and 1000 Oe.

presence of strontium hexaferrites ($SrFe_{12}O_{19}$) [20]. Such precipitation was observed by Anita Fossdal et al., where the authors justified the existence of $SrFe_{12}O_{19}$ based on ternary phase diagram La_2O_3–Fe_2O_3–SrO [21]. This interpretation is in a good agreement with the magnetization data which yielded a transition temperature of $T_C = 700$ K typical of strontium hexaferrites.

4. Conclusions

$La_{1-x}Sr_xFeO_{3-\gamma}$ perovskites with different concentrations of Sr have been successfully prepared by using a sol gel method. XRD results showed that the samples can either have orthorhombic and rhombohedral structures. The average crystallite size was found to decrease with the increasing concentration for $0 \leqslant x \leqslant 0.4$. Mössbauer spectra for the sintered $LaFeO_3$ sample showed a typical antiferromagnetic ordering where the number of Fe^{3+} sites prevails over the Fe^{4+} sites. Moreover, the Mössbauer hyperfine parameters for the calcined samples revealed that the number of Fe^{3+} sites decreases for increasing concentration of Sr. The rearrangements of the ions in the crystallographic sites due to the sintering process were found to influence the magnetic properties. The sintering process increase the Fe^{4+} decrease the paramagnetic sites. Magnetization measurements also showed that the magnetization measured at the highest applied magnetic field is also influenced by the concentration of Sr. The enhancement in the coercivity and in the saturation magnetization for the calcined and sintered samples of $La_{0.6}Sr_{0.4}FeO_{3-\gamma}$ may be associated with the presence of a small amount of strontium hexaferrite.

Acknowledgments

This work was partially supported by the Brazilian agencies CNPq, FACEPE, FINEP, CAPES.

References

[1] Javier Blasco, Bartolomé Aznar, Joaquín García, Gloria Subias, Javier Herrero-Martín, Jolanta Stankiewicz, Phys. Rev. B 77 (2008) 054107.
[2] R.J. McQueeney, J. Ma, S. Chang, J.-Q. Yan, M. Hehlen, F. Trouw, Phys. Rev. Lett. 98 (2007) 126402.
[3] F. Gao, P.L. Li, Y.Y. Weng, S. Dong, L.F. Wang, L.Y. Lv, K.F. Wang, J.-M. Liu, Appl. Phys. Lett. 91 (2007) 072504.
[4] T. Ishikawa, S.K. Park, T. Katsufuji, T. Arima, Y. Tokura, Phys. Rev. B 58 (1998) 20.
[5] Daniel D. Taylor, Nathaniel J. Schreiber, Benjamin D. Levitas, Xu. Wenqian, Pamela S. Whitfield, Efrain E. Rodriguez, Chem. Mater. 28 (2016) 3951–3960.
[6] Victor L. Kozhevnikov, Ilia A. Leonidov, Mikhail V. Patrakeev, Alexey A. Markov, Yakov N. Blinovskov, J. Solid. State Electrochem. 13 (2009) 391–395.
[7] C. Batiot-Dupeyrat, F. Martinez-Ortega, M. Ganneb, J.M. Tatibouët, Appl. Catal. A: General 206 (2001) 205–215.
[8] J.B. Goodenough, Magnetism and The Chemical Bond, Interscience Publishers, New York, 1963.
[9] M. Eibschütz, S. Shtrikman, D. Treves, Phys. Rev. 156 (1967) 2.
[10] M. Takano, T. Okita, N. Nakayama, Y. Bando, Y. Takeda, O. Yamamoto, J.B. Goodenough, J. Solid State Chem. 73 (1988) 140–150.
[11] Jiangong Li, Xinli Kou, Yong Qin, Haiying He, Phys. Status Sol. (a) 191 (1) (2002) 255–259.
[12] T. Mizokawa, A. Fujimori, Phys. Rev. Lett. 80 (1998) 6.
[13] M. Takano, J. Kawachi, N. NAkanishi, Y. Taked, J. Solid State Chem. 39 (1981) 75–84.
[14] J. Matsuno, T. Mizokawa, A. Fujimore, Y. Takeda, S. Kawasaki, M. Takano, Phys. Rev. B 66 (2002) 193103.
[15] R.B. da Silva, J.H. de Araújo, J.M. Soares, F.L.A. Machado, J. Appl. Phys. 115 (2014) 113906.
[16] L. Lutterotti, Maud (material analysis using diffraction), in: Proceeding of the Twelfth International Conference on Textures of Materials (ICOTOM-12), vol. 1, 199, p. 1599.
[17] S.E. Dann, D.B. Currie, M.T. Weller, J. Solid State Chem. 109 (1994) 134–144.
[18] J.B. Yang, W.B. Yelon, W.J. James, Phys. Rev. B 66 (2002) 184415.
[19] J.T. Phong, D.H. Manh, L.H. Nguyen, D.K. Tung, N.X. Phuc, I.-J. Lee, J. Magn. Magn. Mater. 368 (2014) 240–245.
[20] Z.F. Zi, Y.P. Sun, X.B. Zhu, Z.R. Yang, J.M. Dai, W.H. Song, J. Magn. Magn. Mater. 320 (2008) 2746–2751.
[21] Anita Fossdal, Mari-Ann Einarsrud, Tor Grande, J. Am. Ceram. Soc. 88 (2005) 1988–1991.